

RESEARCH ARTICLE | JUNE 03 2024

# Engraved complementary toroidal metasurfaces for potential energy harvesting applications in microwave band

G. Fanourakis  ; P. Markaki; A. Theodosi ; O. Tsilipakos ; Z. Viskadourakis  ; G. Kenanakis  

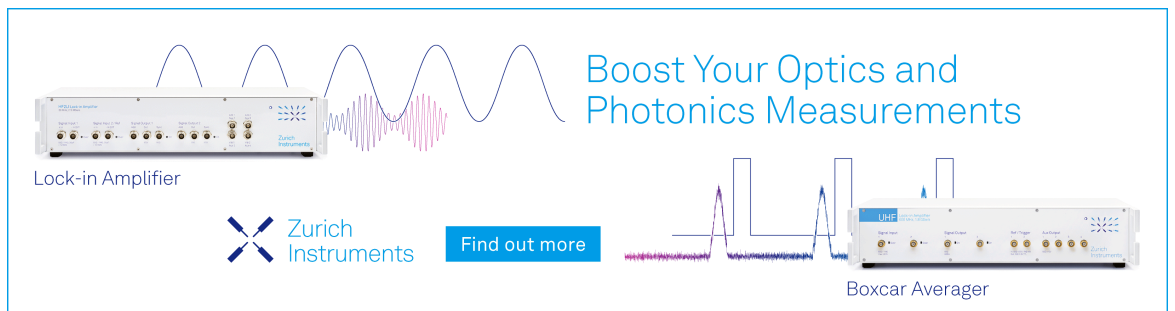
 Check for updates

*J. Appl. Phys.* 135, 213101 (2024)

<https://doi.org/10.1063/5.0190763>


  
View  
Online

  
Export  
Citation



Boost Your Optics and Photonics Measurements

Lock-in Amplifier

 Zurich Instruments

[Find out more](#)

Boxcar Averager

# Engraved complementary toroidal metasurfaces for potential energy harvesting applications in microwave band

Cite as: J. Appl. Phys. 135, 213101 (2024); doi: 10.1063/5.0190763

Submitted: 8 December 2023 · Accepted: 14 May 2024 ·

Published Online: 3 June 2024



G. Fanourakis,<sup>1,a)</sup> P. Markaki,<sup>2</sup> A. Theodosi,<sup>1</sup> O. Tsilipakos,<sup>3</sup> Z. Viskadourakis,<sup>1,b)</sup> and G. Kenanakis<sup>1,b)</sup>

## AFFILIATIONS

<sup>1</sup>Institute of Electronic Structure and Laser (IESL), Foundation for Research and Technology—Hellas (FORTH), N. Plastira 100, Vassilika Vouton, Heraklion GR-70013, Greece

<sup>2</sup>Physics Department, University of Crete, Vassilika Vouton, Heraklion GR-70013, Greece

<sup>3</sup>Theoretical and Physical Chemistry Institute, National Hellenic Research Foundation, Athens GR-11635, Greece

<sup>a)</sup>Present address: Department of Electronics and Nanoengineering, School of Electrical Engineering, Aalto University, 02150 Espoo, Finland

<sup>b)</sup>Authors to whom correspondence should be addressed: zach@iesl.forth.gr and gkenanak@iesl.forth.gr

## ABSTRACT

In the current study, complementary metasurface units with toroidal geometry were fabricated, using the computer numerical control engraving method. The metasurfaces were engraved in copper-coated, FR-4 plates. The produced metasurfaces were electromagnetically characterized in the microwave regime. Furthermore, they were studied regarding their energy harvesting capability, in the microwave range, where they absorb electromagnetic energy. It was found that toroidal structures harvest energy from the incident microwaves and transform it to electric power, through a simple rectification circuit. Moreover, their energy harvesting efficiency was found to be comparable or even superior to those of others reported so far. Therefore, the hereby obtained experimental results evidently show that engraved toroidal metasurfaces could potentially be used as energy harvesters in the microwave regime.

© 2024 Author(s). All article content, except where otherwise noted, is licensed under a Creative Commons Attribution (CC BY) license (<https://creativecommons.org/licenses/by/4.0/>). <https://doi.org/10.1063/5.0190763>

## I. INTRODUCTION

Metamaterials (as well as their two-dimensional counterparts called metasurfaces) can be defined as artificial materials composed of periodically arranged subwavelength resonant meta-atoms. They possess exotic electromagnetic properties, such as negative to largely positive values of refractive index and artificial magnetism at high frequencies, etc.<sup>1–6</sup> Due to those extraordinary properties, metamaterials and metasurfaces have been exploited for numerous applications including perfect absorption and electromagnetic shielding, sensing, polarization control, anomalous reflection/refraction and beam splitters, optical stirring, and broadband delay devices, to name a few.<sup>7–14</sup> Lately, metamaterials and metasurfaces have been realized for energy harvesting applications,<sup>15–18</sup> in a wide frequency range. In particular, special attention has been paid to metasurfaces operating in the microwave regime. The advantage of

such metasurfaces is that they have dimensions of a few millimeters and can be developed in a relatively easy manner, employing conventional methods, such as those used in the development of electronic circuits or thin film devices. Nevertheless, the exploding interest of microwave metasurfaces in energy harvesting applications mainly stems from the dramatical growth of microwave wireless networks,<sup>19,20</sup> which are used mostly for wireless telecommunications. Large amount of microwave power is emitted from antennas and wi-fi hubs, while only a fraction of that is received and converted into signal. Therefore, the tremendous growth of wireless networking also generates a significant amount of wasted energy, which is considered as the energy source for microwave energy harvesters.

Thus far, there are numerous metasurface designs proposed, exhibiting high harvesting performance in the microwave

03 June 2024 09:26:02

regime.<sup>6,16</sup> Various shapes and configurations have been proposed, such as split ring resonators (SRRs),<sup>21,22</sup> cut-wire meta-atoms,<sup>23,24</sup> cross-shaped resonators,<sup>18,25</sup> and rectangular or circular ring resonators.<sup>26,27</sup> Moreover, complementary metasurfaces (where the geometry is carved into an otherwise uniform metallic film) have also been proposed for energy harvesting.<sup>21,22,27–29</sup>

Regardless of their shape and configuration, microwave metasurfaces are usually constructed by employing typical the printed circuit board (PCB) technology, allowing for the production high quality metasurface units. PCBs can be defined as rugged nonconductive boards built on substrate-based structures. They are prevalent in electronic devices and can be easily identified as the green-colored board in most cases. Based on the design specifications and requirements, many active (for example, operational amplifiers and batteries) and passive components (such as inductors, resistors, and capacitors) are mounted on the PCBs to match the form factor of the final design.<sup>30</sup>

Although, the PCB process is a well-established, industry-oriented technology, used for the manufacturing of electronic circuits and components, it requires a complex procedure to ensure the performance of the finished product, such as lamination Cu/polymer, PCB fabrication, component assembly using conductive adhesives, encapsulation of the circuit, thermoforming, heating and sagging of the electronics circuits, forming using the desired mold designs, etc., reaching 20 or even more steps during manufacturing.<sup>30,31</sup> Therefore, such a process is not that user-friendly, especially for the development of metasurfaces in the laboratory. Moreover, the core or inner layers of the printed circuit boards need to have extra copper removed before the PCB fabrication process can continue. Etching involves covering the necessary copper on the board and exposing the rest of the board to a chemical. The chemical etching process removes all unprotected copper from the PCB, leaving only the board's necessary amount. The latter process shows that, in several cases, the PCB process is not so environmentally friendly, as it involves chemicals, acids, and flammable or even toxic reagents.<sup>32</sup>

On the other hand, energy harvesting metasurfaces have been successfully grown, using more versatile routes, such as fused filament fabrication (FFF).<sup>24</sup> This is a three-dimensional printing technique, using a polymer composite as a starting material. Such a method is simpler, cheaper, user-friendly, as well as laboratory-oriented, compared to the PCB method. The main drawback of the method is that the produced metasurfaces exhibit relatively low electrical conductivity, leading to reduced harvesting efficiency.

Alternately, the fabrication of complementary metasurfaces employing the so-called Computer Numerical Control (CNC) method has been recently reported.<sup>33</sup> CNC milling is a subtractive fabrication process that uses rotating cutting tools to remove materials from a starting stock piece, commonly referred to as the workpiece. The CNC milling system typically consists of a worktable for positioning the workpiece, a cutting tool (most commonly an endmill), and an overhead spindle for securing and rotating the cutting tool. CNC helps to automate the fabrication process, thus improving repeatability and precision, reducing human error, and adding advanced capabilities (e.g., the direct conversion of CAD models to finished parts).<sup>34</sup> Moreover, the CNC process does not

involve the use of chemicals, which are demanded in other manufacturing processes, making it particularly advantageous for printed circuit boards.<sup>35,36</sup>

Although the CNC process is quite promising compared to PCB technology, there are some limitations that must be taken into account. Those limitations are mostly related to the resolution and the accuracy of the engraving process. In practice, the resolution and the accuracy of the CNC engraving method depends on several parameters, such as cutting tools used, CNC cutting speed, the dimensions, as well as the complexity of the engraved object itself, the surface used for engraving, etc.<sup>37–39</sup> Considering all those parameters, the resolution of the CNC engraving process could go down to a few tens of micrometers. Such high resolution/accuracy levels are achieved only when optimal engraving conditions are presumed. However, the CNC engraving method still exhibits fair accuracy and resolution compared to methods previously discussed.

In the current study, the CNC method is employed to develop complementary metasurfaces, with a toroidal geometry [i.e., Fig. 1(a)], on metallized surfaces. Such a metasurface topology has been chosen since it exhibits strong resonant response, which can be gently manipulated, by tuning the dimensions of the central gap.<sup>40</sup> Therefore, an efficient harvesting performance could be expected. Notably, metasurfaces with such a geometry have been studied previously, regarding their energy harvesting response.<sup>41–43</sup> In particular, arrays of metasurfaces with the toroidal topology have exhibited high harvesting efficiency and insensitivity to the incident angle. Nevertheless, complementary toroidal metasurfaces (CTMs) have not been studied, to the best of our knowledge. Moreover, compared to other approaches alternative to PCB, the CNC method is easier than FFF printing and dedicated for large-scale production, enabling the production of metasurface sensors in the industrial scale. Therefore, the utilization of such methods to develop metasurfaces for energy harvesting sounds a rather promising approach.

Therefore, CTMs similar to those previously investigated<sup>40</sup> were developed employing the CNC method, combined with a router, dedicated to engrave surfaces, such as metals, wood, and polymers. In the current study, CTMs were being fabricated on metallized FR-4 surfaces. All fabricated CTMs were characterized regarding their electromagnetic (EM) performance, so as their efficient absorbing behavior is confirmed. By appropriately incorporating a Schottky diode, the basic rectification process took place and corresponding DC signals were recorded. Various experiments were performed in order to clarify the intrinsic nature of the observed signals, as well as optimum conditions needed so as the whole setup shows maximum output power and harvesting efficiency. It is shown that the studied CTMs exhibit a rather good energy harvesting performance, showing efficiencies of the order of 30%, in the frequency range around 4–4.5 GHz, enabling the capability of such structures to be used for energy harvesting applications in the microwave regime.

## II. EXPERIMENTAL DETAILS

A unit cell of toroidal topology is investigated in the current study [Fig. 1(a)]. In its conventional form, the toroidal structure exhibits a very sharp and controllable electromagnetic response,<sup>40</sup>

03 June 2024 09:26:02

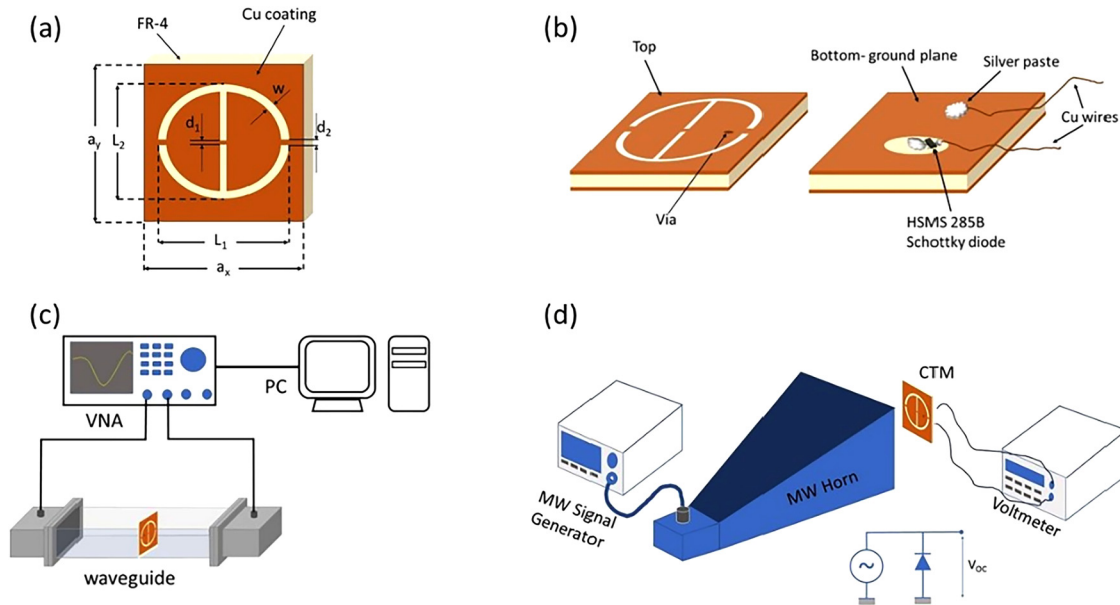


**FIG. 1.** (a) Drawing of the complementary toroidal metasurface. Dimensions are also shown. (b) Topography of the metasurface, showing the via interconnect and the connection of the diode between the top surface and the ground plane. (c) Experimental setup of the electromagnetic characterization of the engraved metasurfaces. (d) Experimental setup, dedicated for energy harvesting experiments. The equivalent electronic circuit is also presented.

enabling its promising potential for efficient energy harvesting. Mechanical engraving was used in order to develop such metasurfaces, using a home-built CNC router. The appropriate drawings of the metasurfaces were developed using the open-source CAD software EASEL (Inventables Inc., Chicago, IL, USA, <https://site.inventables.com/technologies/easel>). The same software was used to transform the CAD file to the corresponding g-code files as well as to guide the CNC router. The router moved in all three dimensions upon engraving with a thin metallic carpenter blade (diameter:  $\varnothing$  1.0 mm). The substrate/material, at the top of which the desired metasurfaces were developed, was a typical plain FR-4 surface (1.5 mm thick), covered with a  $35\mu\text{m}$ -thick copper cladding. During the process, the blade removed certain areas of the Cu film; thus, the final complementary metasurface was formed [see Fig. 1(a)—from now on this structure will be referred to as CTM1]. The depth of the engraved structures was kept at 0.2 mm. Another toroidal metasurface was also developed on the double-sided Cu-coated FR-4 surface [Fig. 1(b)], with the bottom coating acting as the ground plane (this structure will be referred to as CTM2).

The produced metasurfaces were investigated regarding their dimensions via optical microscopy experiments. For this reason, an optical microscope was used (AP-8 microscope, Euromex Microscopen bv., Arnhem, the Netherlands), with the maximum magnification of  $\times 80$ . Both desired and measured dimensions of all metasurfaces are listed in Table I.

The electromagnetic response of the engraved metasurfaces was investigated via S-parameter measurements in the microwave regime. In particular, all engraved structures were measured using a combination of a P9372A vector network analyzer (VNA)

(Keysight, CA, USA) and WR187 waveguide [i.e., Fig. 1(c)]. Details regarding the setup and the measurement procedure were previously described.<sup>24,44</sup>

In order to investigate the energy harvesting performance of the complementary metasurfaces, a modified configuration proposed by Alavikia *et al.*<sup>21,22</sup> is employed. In particular, a via interconnect (0.5 mm diameter) is made through the dielectric slab, as shown in Fig. 1(b). In the ground plane side, the copper coating around the via has been removed in order to exclude any possibility of short circuit between the top coating and the ground plane. Moreover, a HSMS 285B Schottky diode was connected between the via and the ground plane, for rectification purposes. Schottky

**TABLE I.** Nominal and measured dimensions of the studied complementary metasurfaces.

	Toroidal meta-atom dimensions	
	Nominal values (mm)	Measured values (mm)
$a_x$	24.7	$24.6 \pm 0.3$
$a_y$	22.5	$22.0 \pm 0.2^a$
$L_1$	24.0	$24.1 \pm 0.2$
$L_2$	22.0	$22.0 \pm 0.2^a$
$w$	3.30	$3.3 \pm 0.1$
$d_1$	0.80	$0.61 \pm 0.03$
$d_2$	1.20	$0.96 \pm 0.04$

<sup>a</sup>Dimensions  $a_y$  and  $L_2$  are fixed to the width of the WR187 waveguide.

diodes of the same family have been successfully used for microwave signal rectification, in several previous works.<sup>45–47</sup> The DC voltage drop measured across the diode is considered as the voltage output harvested by the device. The same configuration is also employed in all complementary metasurfaces, studied here, regardless the presence/absence of the ground plane.

The above-described device was placed in front of a horn antenna and in the middle of its cross section. The horn is connected to a microwave signal generator, transmitting electromagnetic waves in the range 9 kHz–6 GHz, with a maximum power of ~0.5 W. The voltage drop across the diode is measured, through a sensitive voltmeter. Using this experimental setup, the DC output signal as a function of frequency is recorded. Moreover, the DC output signal is also recorded with respect to the horn power, upon constant frequency. Furthermore, corresponding experiments were performed, with respect to the orientation of the metasurface against the horn. The experimental setup is shown in Fig. 1(d).

At this point, it has to be stressed that the above described experimental setup and procedure have been successfully used in a previous investigation, concerning the energy harvesting performance for 3D printed metasurfaces.<sup>24</sup> Compared to other reports,<sup>45,48–51</sup> in which clusters of metasurfaces are placed several meters away from the horn, it exhibits distinct advantages. Especially in the case where the energy harvesting device consists of a single unit (such as in our case), the produced DC output signal is expected to be rather weak. Thus, by putting the device next to the horn, the metasurface absorbs more energy, which results in producing stronger output voltages. Moreover, such experiments were performed in open space, thus several parasitic signals could contribute to the measured DC output signal. Hence, placing the metasurface in front of the horn is a rather simple and appropriate route to enhance the signal-to-noise ratio, resulting in the further improvement of the measured DC voltage. Moreover, regarding the rectification process, it has to be noted that traditional low-frequency rectifiers consisting of a diode in series with a resistor–capacitor pair fail to rectify microwave signals because the capacitor is by-passed, and the RC component cannot filter the time-varying component of the original signal. However, a simple microwave rectifier can consist of a diode and considered as a resonance circuit exhibiting its best performance in the desired frequency regime.<sup>52</sup> Due to its simplicity, this rectification circuit will probably suppress the overall performance of the harvesting device. However, the optimization of the microwave-to-DC conversion in such devices is a wide and intriguing field of investigation, and falls out of the scope of the current study.

Theoretical simulations were also performed. In particular, full-wave simulations with a continuous wave (CW) excitation were performed using the frequency domain solver of the commercial software CST Studio Suite. The toroidal meta-atom was engraved on a double copper-coated FR-4 substrate and then the whole structure was inserted in the center of the WR187 waveguide. In addition, rectangular waveguide ports were used to excite the structure with the fundamental,  $TE_{10}$  mode of the waveguide. The waveguide walls were considered to be perfect electric conductors (PECs) through the PEC boundary conditions. Copper top and bottom layers were modeled via the electric conductivity of  $5 \times 10^7$  S/m for these frequencies.

The relative electric permittivity of the FR-4 substrate considered to be 4–0.04i. An automatic adaptive mesh refinement procedure was followed to obtain converged results for the S parameters.

### III. RESULTS AND DISCUSSION

Figure 2(a) shows a typical picture of the developed complementary toroidal metasurface (CTM1). It seems that the structure is well engraved into the Cu-coated FR-4 substrate. Lines are straight, with parallel edges [Fig. 2(b)]. Corners are a bit rounded [Figs. 2(c) and 2(d)], which is most likely attributed to the engraving process as well as to the engraving blade used. Moreover, well-defined gaps [Figs. 2(c) and 2(d)] are shown, although their corners are also rounded. The dimensions of the metasurface are listed in Table I. Long dimensions  $L_1$  and  $L_2$  are in good agreement with the theoretical values. Here, it must be noted that both  $a_y$  and  $L_2$  dimensions of the toroidal metasurface are kept at approximately 22 mm, so that the device can be fitted into the WR187 waveguide (i.e., width 22.4 mm).

Regarding the line width  $w$  dimensions, measured values are identical to the desired ones, while gap dimensions  $g_1$  and  $g_2$  are smaller than the corresponding nominal values. Therefore, the CNC engraving process results in the development of well-shaped complementary metasurface units; however, fine tuning of the process is required in order to achieve the exactly desired dimensions.

The electromagnetic response of the engraved metasurface units is shown in Fig. 3. In particular, Fig. 3(a) shows the  $S_{21}$

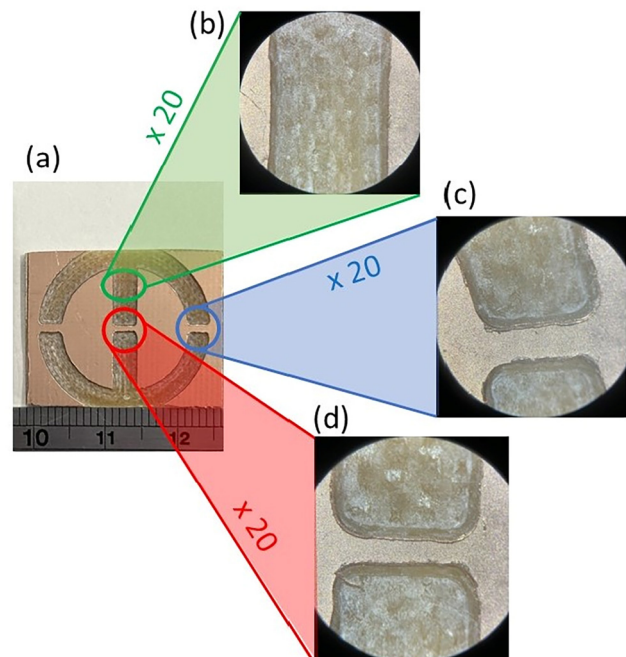
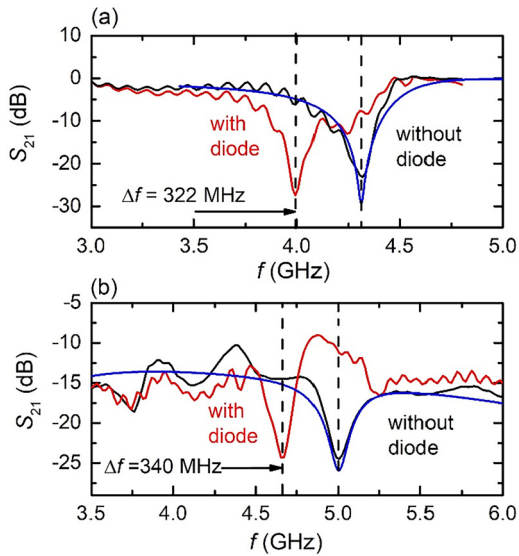


FIG. 2. (a) Typical picture of the engraved toroidal meta-atom. Optical microscopy pictures (b)–(d) reveal details of the engraved structure.



**FIG. 3.** (a) Transmittance spectrum for the CTM1 sample with (red line) and without (black line) the diode included. (b) Transmittance spectrum for the CTM2 sample. Black line corresponds to electromagnetic response without diodes, while the red line corresponds to the electromagnetic signal with diodes. In both panels, blue solid line corresponds to spectra extracted from theoretical simulations.

parameter (black solid line) as a function of frequency, for the CTM1 structure. A sharp dip is observed at 4.3 GHz. The dip is indicative of negligible transmission observed at this certain frequency. Moreover, the  $S_{11}$  vs  $f$  spectrum shows a distinct drop at the same frequency, suggestive of negligible reflection [Fig. S1(a) in the supplementary material]. In general, transmission  $T = |S_{21}|^2$ , reflection  $R = |S_{11}|^2$ , and absorption  $A$  are interconnected through the relation

$$A + R + T = 1. \quad (1)$$

Considering the almost zero transmission and reflection, observed at the resonance frequency, it can be concluded that the CMT1 fully absorbs the incident electromagnetic energy, when in resonance. Furthermore, the resonance frequency and the basic characteristics of the  $S_{21}$  vs  $f$  spectrum are consistent with predicted spectra coming from corresponding theoretical simulations [blue solid line, Fig. 3(a)]. Moreover, the hereby obtained electromagnetic results are in qualitative agreement with results presented for three-dimensional printed toroidal meta-atoms.<sup>40</sup> With the diode included (red solid line), the resonance dip shifts toward lower frequencies; The shift is  $\sim 322$  MHz. A similar resonance shift has been observed for 3D printed cut-wire metasurfaces.<sup>24</sup> In addition, Fig. 3(b) shows the  $S_{21}$  vs frequency for the CTM2 sample. There is a well-defined dip at 5 GHz, which is also predicted from theoretical simulations and it is indicative of absorption at that frequency. The presence of diode shifts the resonance dip by  $\sim 340$  MHz, toward lower frequencies. Both samples are expected to harvest

energy in the frequencies where the metasurface units absorb in the presence of the diode.

The electromagnetic response of the engraved toroidals, with respect to the angle of the incident wave, is of great importance, since it directly affects the absorption of the metasurface and the corresponding energy harvesting in actual operating conditions. There are three different angles that the metasurface can rotate with respect to the incident wave, delta, theta, and phi (i.e., see Fig. S2 in the supplementary material). Nevertheless, due to WR187 waveguide dimension constraints, we can study only the effect of angles theta and phi. The corresponding experimental evidence for the CTM1 sample is shown in Fig. 4. Particularly, Fig. 4(a) shows the evolution of the  $S_{21}$  parameter with respect to the frequency for various theta angles. The resonance frequency shifts to lower values, while the resonance depth is also reduced. We quantify the spectral position and the minimum transmission value in Fig. 4(b). For theta = 90°, resonance almost vanishes, suggesting that the metasurface does not absorb.

On the other hand, Fig. 4(c) shows the  $S_{21}$  vs frequency, against various phi angles. The main dip remains almost stable in the vicinity of 3.9–4 GHz [i.e., see Fig. 4(d)]. Furthermore, the resonance depth decreases with increasing phi, up to 60°, and then it remains almost constant. Interestingly, there are satellite dips revealed as the phi angle increases. Both dips constantly shift toward the main dip, with increasing phi angle [Fig. 4(d)]. Moreover, their depth increases and becomes larger than the main resonance dip for phi greater than 60°. The above-observed complex electromagnetic behavior of the CTM1 sample is fairly reproduced by corresponding numerical simulations (i.e., see Fig. S3 in the supplementary material).

$S_{21}$  vs frequency spectra, upon various theta angles, are presented for the sample CTM2, in Fig. 5(a). The resonance dip at  $\sim 4.7$  GHz, goes towards lower frequencies, and it decreases with increasing theta angle [Fig. 5(b)]. Such behavior is qualitatively similar to the behavior of the CTM1 sample. Simultaneously, a second resonance dip develops at higher frequencies, which also shifts toward the main one, as the theta angle increases [i.e., Fig. 5(c)]. Nevertheless, for theta above 60°, both dips are dramatically suppressed, and they are almost eliminated for 90°. Figure 5(d) shows the  $S_{21}$  vs frequency spectra for the CTM2 sample, upon changing phi angle. The main dip at 4.65 GHz seems to be rigid [Fig. 5(e)]; however, a secondary dip develops and becomes observable above 45°. This dip moves toward higher frequencies [Fig. 5(e)], as the angle phi increases. Moreover, its depth is comparable or even greater than the main one [Fig. 5(f)]. The above-described electromagnetic behavior is qualitatively corroborated with corresponding theoretical simulation results (i.e., see Fig. S4 in the supplementary material).

The above comprehensive electromagnetic response investigation is of great importance since metasurfaces effectively harvest energy, at frequencies where resonance has been observed. In this context, Fig. 6(a) shows open circuit voltage  $V_{OC}$  against frequency, for the CTM1 sample. A clear and well-defined voltage maximum is observed at 3.95 GHz. The peak is at the frequency regime, where corresponding electromagnetic resonance occurs ( $\sim 4$  GHz). At its peak  $V_{OC} = 1.72$  V, while FWHM  $\sim 380$  MHz. The measured voltage indicates the energy harvesting behavior of the metasurface

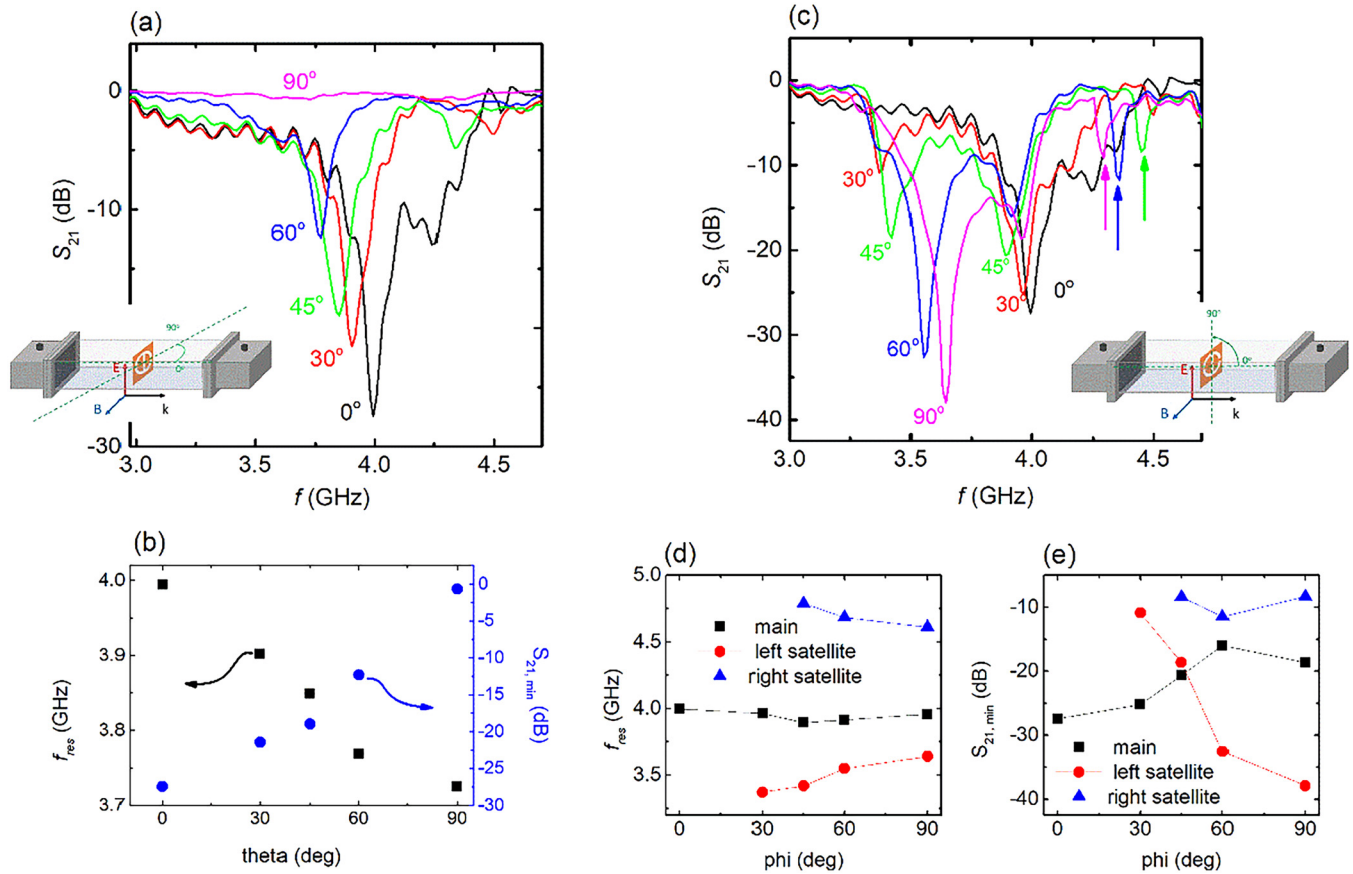


**FIG. 4.** CTM1 sample; (a)  $S_{21}$  vs frequency for various theta angles. The inset shows the experimental configuration used for those measurements. (b) Corresponding resonance frequency (black rectangles) and  $S_{21, \min}$  values (blue circles) with respect to the theta angle, as extracted from panel (a). (c)  $S_{21}$  vs frequency for various phi angles. The satellite dips evolved, with increasing phi, are clearly seen to the left as well as to the right of the main peak. Experimental setup is shown in the inset (d). Corresponding resonance frequency and  $S_{21, \min}$  values, for the main dip, with respect to the theta angle, as extracted from panel (c). (e) Corresponding resonance frequency and  $S_{21, \min}$  values, for both secondary dips, with respect to the phi angle. Solid lines are guides to the eye.

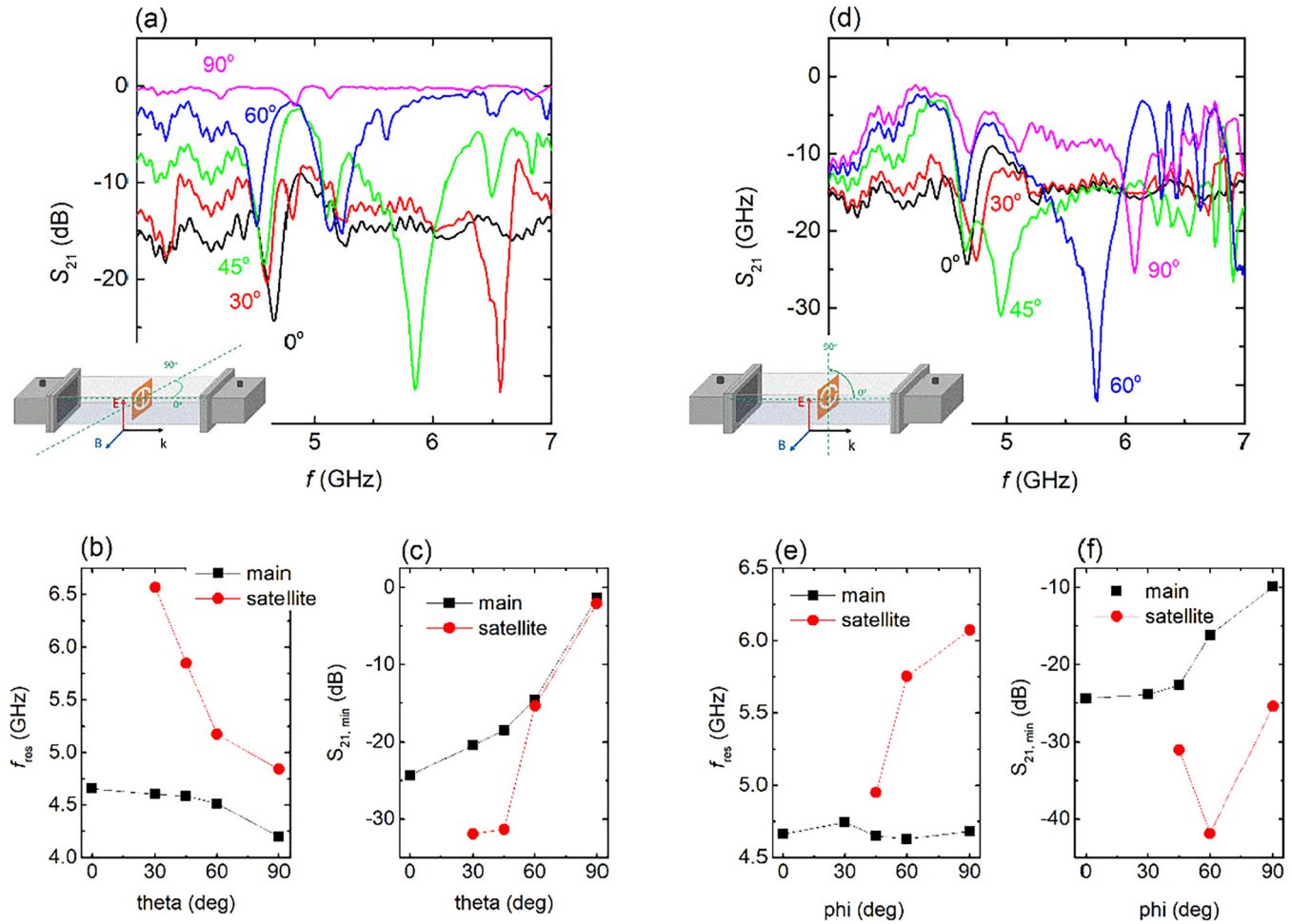
03 June 2024 09:26:02

(the  $\sim 50$  MHz difference between electromagnetic and voltage measurements could be plausibly attributed to the different experimental setups used). The  $V_{OC}$  vs frequency curve is wavy, which can be attributed to the presence of the diode. In general, diodes are non-linear electronic components, which can trap high frequency harmonic modes, other than the fundamental. Such a harmonic mode trapping could result in the curvy character of the open circuit voltage. Moreover, other voltage shoulders are also observed, i.e., at  $\sim 4.7$  GHz. However, their presence does not seem to affect the overall performance of the metasurface.

Confirmation of the intrinsic nature of the observed phenomenon requires further experimental investigation. Figure 6(b) shows the  $V_{OC}$  behavior with respect to the microwave power coming out of the horn. It is seen that  $V_{OC}$  increases, with increasing horn power and for maximum power (24 dBm) we find  $V_{OC} \sim 1.72$  V. Although not directly observed,  $V_{OC}$  seems to saturate above 24 dBm (we cannot perform experiments in higher

power levels due to horn power generator constraints). Such dependence of the open circuit voltage with respect to the horn power, indicates the energy harvesting function of the metasurface. Moreover, such behavior is indicative that the investigated metasurface reaches its maximum harvesting capability. On the other hand, Fig. 6(c) depicts the harvesting response of the metasurface, when horn power is set on and off. It is clearly seen that  $V_{OC}$  takes non-zero values when the horn power sets on (“ON” mode), depending on the power level.  $V_{OC}$  becomes zero, as soon as the power is interrupted (“OFF” mode). Furthermore, when in the “ON” mode,  $V_{OC}$  is extremely constant, with respect to time, i.e., Fig. 6(d). All the above experimental evidence demonstrates the capability of the toroidal metasurface to transform the microwave energy to electrical power. Therefore, complementary toroidal metasurface could harvest energy in the microwave band.

Such an important observation merits further investigation, i.e., it is sensible to study the energy harvesting capability with



03 June 2024 09:26:02

**FIG. 5.** CTM2 sample; (a)  $S_{21}$  vs frequency for various  $\theta$  angles. A secondary dip evolved, with increasing  $\phi$ , and it is clearly seen to the right of the main peak. Experimental setup is shown in the inset (b). Corresponding resonance frequencies and (c)  $S_{21, \min}$  values with respect to the  $\theta$  angle, as extracted from panel (a), for both dips (d)  $S_{21}$  vs frequency for various  $\phi$  angles. The satellite dip evolved, with increasing  $\phi$ , is clearly seen to the right of the main peak. Experimental setup is shown in the inset (e). Corresponding resonance frequencies and (f)  $S_{21, \min}$  values, for both the main and satellite dips, with respect to the  $\theta$  angle, as extracted from panel (c). Solid lines are guides to the eye.

respect to the incident angle. It has been previously shown that the electromagnetic response of the metasurface is directly affected by such factors. Therefore,  $V_{OC}$  vs frequency experiments, for various  $\theta$  and  $\phi$  angles are performed for the CTM1 sample (Fig. 7). More specifically, the  $V_{OC}$  vs  $f$  behavior, with respect to the  $\theta$  angle, is depicted in Figs. 7(a) and 7(b). Upon increasing  $\theta$ ,  $V_{OC}$  peak shifts to lower values, as well as peak value dramatically decreases. Even more, the  $V_{OC}$  vs  $f$  behavior, with respect to the  $\phi$  angle, is shown in Figs. 7(c) and 7(d). Here, the resonance frequency remains unaffected, with increasing  $\phi$ , nonetheless corresponding voltage value decreases. Moreover, a secondary voltage peak shows up and shifts toward the main one, for angles greater than  $45^\circ$ . Such a harvesting performance follows closely the corresponding electromagnetic behavior shown in Fig. 4 and strongly

indicates that harvesting capability of the metasurface is directly affected by the incident wave. From the practical point of view, the metasurface harvests energy in a more efficient manner as long as the incident wave hits its surface vertically. Additionally, it seems that the secondary voltage peak qualitatively agrees with the secondary  $S_{21}$  minimum shown in Fig. 4(c); therefore, it cannot be considered as an artifact.

Since the harvesting performance of the metasurface has been verified and connected to its corresponding electromagnetic behavior, it is crucial to investigate the efficiency of the metasurface. In this context, we connected several different resistances, in parallel to the diode and we recorded the output voltage  $V_{OUT}$  as a function of frequency. Corresponding results are shown in Fig. 8(a). It is seen that  $V_{OUT}$  increases with increasing  $R$ , reaching the  $V_{OC}$  value



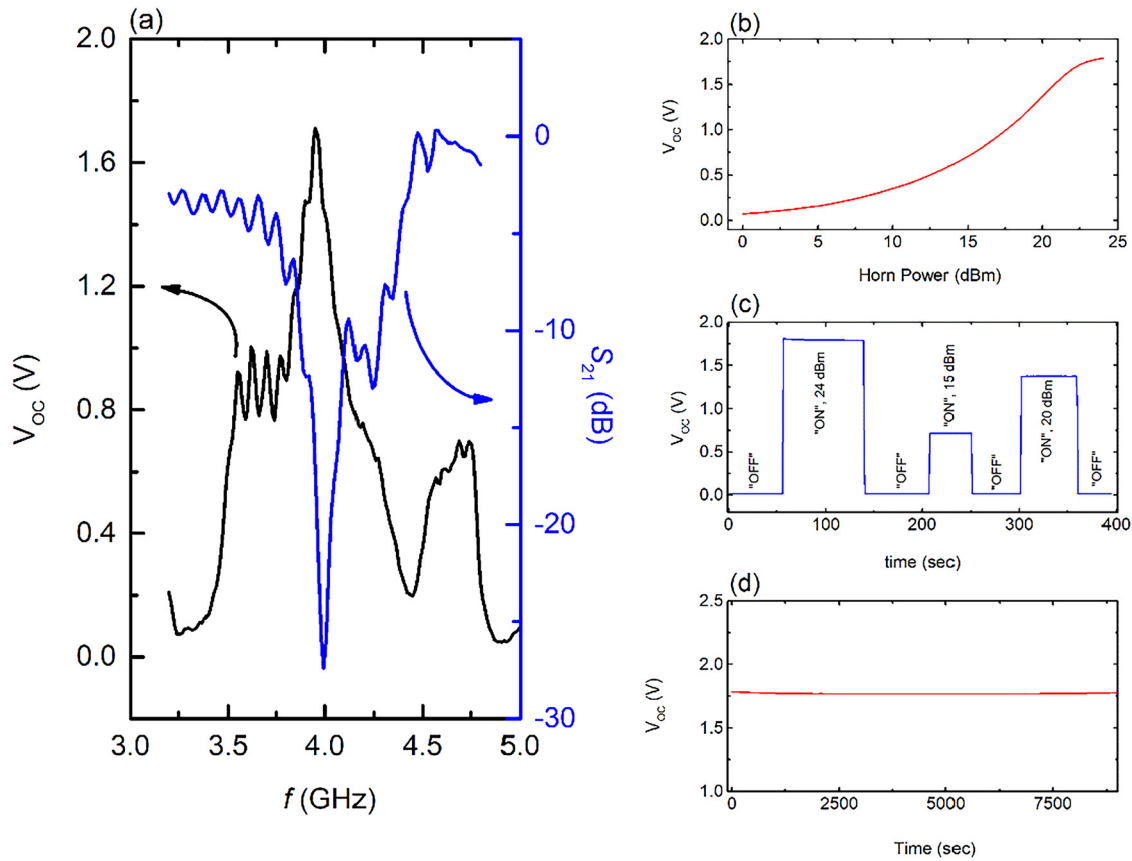
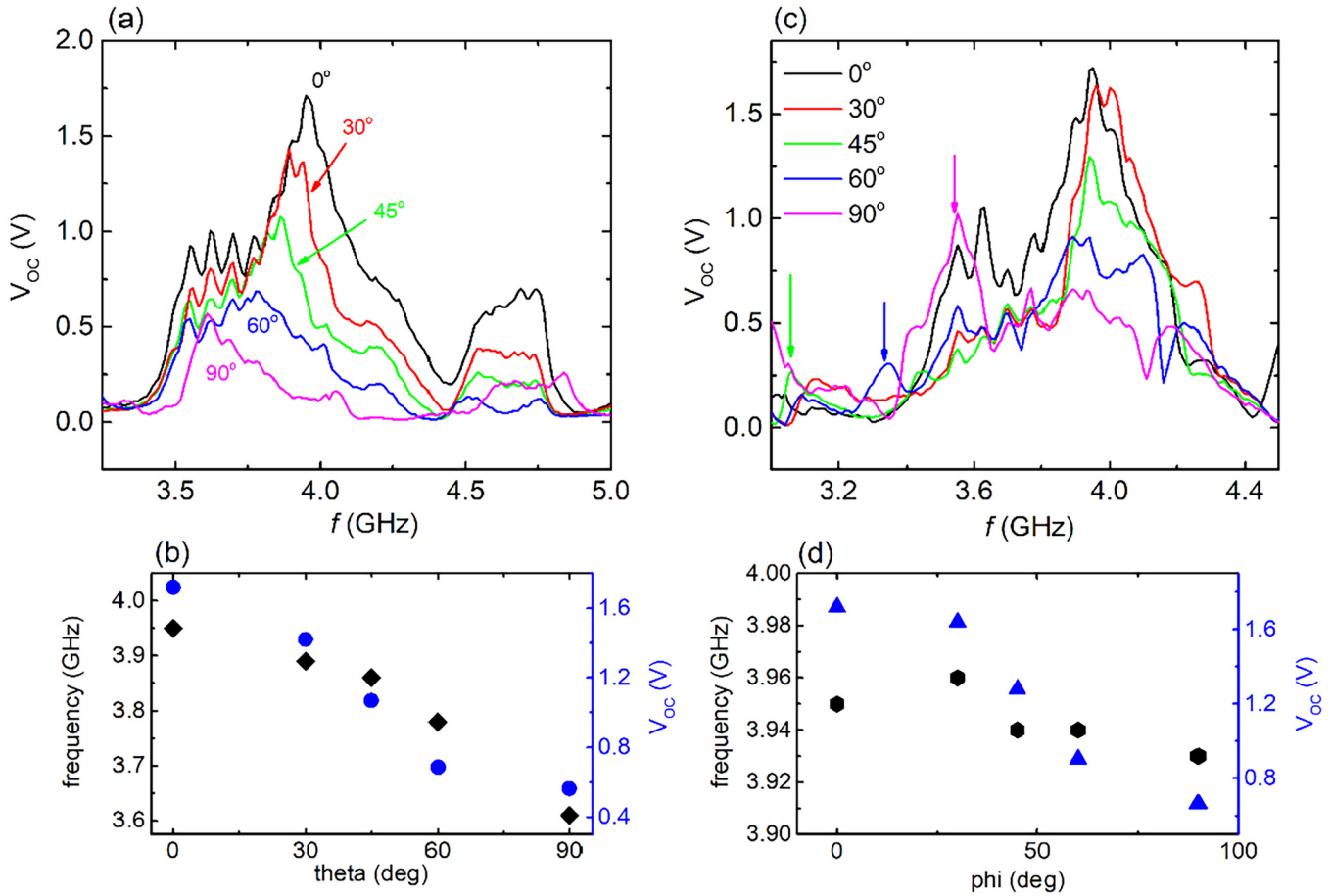


**FIG. 6.** (a) Open circuit voltage vs frequency for the CMT1 sample (black line). A clear peak is observed at the frequency where the metasurface absorbs (blue line). (b)  $V_{OC}$  as a function of horn power ( $f = 3.95$  GHz). (c)  $V_{OC}$  behavior, with respect to “ON” and “OFF” status of the horn power. (d)  $V_{OC}$  measured with respect to time in the “ON” state.

for resistance loading greater than  $\sim 500$  k $\Omega$  [Fig. 8(b)]. The  $V_{OUT}$  peak value is observed at 3.95 GHz for all resistance loadings. Considering the  $V_{OUT}$  values, the output power of the harvesting device can be calculated through the relation  $P_{OUT} = V_{OUT}^2/R$ , and the results are presented in Fig. 8(c). A clear maximum is obtained ( $\sim 2$  mW) for 200  $\Omega$ , suggesting that the maximum output power can be given for such an external loading. Nevertheless, the  $V_{OUT}$  vs R curve is relatively wide, and power levels near the peak value can be achieved for resistances laying in the vicinity of 100–500  $\Omega$ . From the application point of view, this is a useful result, demonstrating that the device can be potentially used in combination with other electronic devices with overall resistance load of a few hundred Ohms, without losing much of its efficiency. Furthermore, the efficiency of the harvesting device is shown in Fig. 8(d). In order to estimate  $\eta\%$ , we work as follows: the overall power coming out of the horn is 24 dBm = 0.251 W. Assuming that the electromagnetic power exhibits a uniform distribution pattern at the exit of the horn,<sup>53</sup> we put the harvesting device just in front of the horn, and we consider that the power captured by the metasurface unit can be roughly estimated as proportional to the ratio

$A_{MS}/A_{Horn}$ , where  $A_{MS}$  is the surface of the metasurface unit and  $A_{Horn}$  is the cross section of the horn. The horn cross section is 212.5 cm<sup>2</sup>, while the effective area of the metasurface is 5.33 cm<sup>2</sup>. It can be found that the metasurface covers the 2.5% of the total horn area; therefore, it presumably absorbs  $\sim 2.5\%$  of the total horn power. Here, it must be stressed that the metasurface unit captures almost all the incident electromagnetic energy, as evidently proven by corresponding electromagnetic measurements, previously shown. Thus, the incident power is  $P_{IN} = 6.27$  mW, and then the efficiency can be determined through the relation  $\eta\% = P_{OUT}/P_{IN}$ . Following the above-described analysis, we found that the devices harvest energy with a maximum efficiency of  $\sim 33\%$ . Apparently, the efficiency of the harvesting device is roughly estimated, by following such a route. In general, the incident power  $P_{in}$  is calculated employing the equation  $DS = P_t \cdot G_t / 4 \cdot \pi \cdot R^2$ , where  $P_t$  is the power transmitted by the horn,  $G_t$  is the horn gain, and  $R$  is the distance between the power source and the sample under test.<sup>54</sup> The above-mentioned equation determines the power density delivered by the horn, at a certain distance away from the horn. Considering that  $P_t = 0.251$  mW (24 dBm),  $G_t$  (@ 4 GHz) = 13 (as

03 June 2024 09:26:02



03 June 2024 09:26:02

**FIG. 7.** (a) Open circuit voltage vs frequency for the CMT1 sample, under different theta angles. (b) Frequency and measured value of the  $V_{OC}$  peak, as a function of theta angle, as extracted from panel (a). (c)  $V_{OC}$  vs frequency for the CMT1 sample, under different phi angles. (d) Frequency and measured value of the  $V_{OC}$  peak, as a function of phi angle, as extracted from panel (c).

given by the horn manufacturer), and  $R = 0.21$  m, the calculated incident power density is  $DS = 5.88$  W/m<sup>2</sup>. Considering the surface area  $A$  of the metasurface, the power captured by the harvesting device is  $P_m = S \cdot A = 3.27$  mW, resulting in a considerably high harvesting efficiency, which probably does not reflect the real performance of the investigated harvesting device. In particular, although the metasurface itself effectively absorbs almost all the incident microwave energy (as previously shown by the corresponding  $S_{21}$  and  $S_{11}$  spectra), the transformation of such energy to electric power is not that effective, because the rectification circuit used is the simplest possible. Therefore, the rectification efficiency is far away from the optimum one, possibly leading to a suppressed overall harvesting efficiency. Hence, it seems more appropriate to follow the rough estimation of the harvesting efficiency, as previously described. As it will be shown later, such a roughly estimated efficiency value is comparable to others previously reported for corresponding metamaterial structures, giving credence to the reliability of the hereby obtained results.

Energy harvesting experiments have also been performed for the CTM2 sample. In particular, the open circuit voltage as a function of frequency is shown in Fig. 9(a). A broad voltage peak is observed at  $\sim 4.6$  GHz (thus at the same frequency where resonance has been obtained), indicating the harvesting behavior of the metasurface unit. Peak voltage value is  $\sim 3.7$  V, with FWHM  $\sim 500$  MHz. Moreover, energy harvesting experiments, for various angles with respect to the incident wave, are also performed. Corresponding results are consistent with the electromagnetic response signals, previously presented (i.e., see Fig. S5 in the [supplementary material](#)), suggesting the maximum harvesting behavior of the metasurface unit, at resonance frequencies, as well as its performance dependence on the incidence wave angle. In addition, the output voltage of the metasurface unit is measured with respect to the resistance loading, as presented in Fig. 9(b). It is seen that the output voltage increases with increasing resistance loading, approaching the open circuit voltage for resistances greater than 1 M $\Omega$ . Such behavior is similar to that previously observed for the

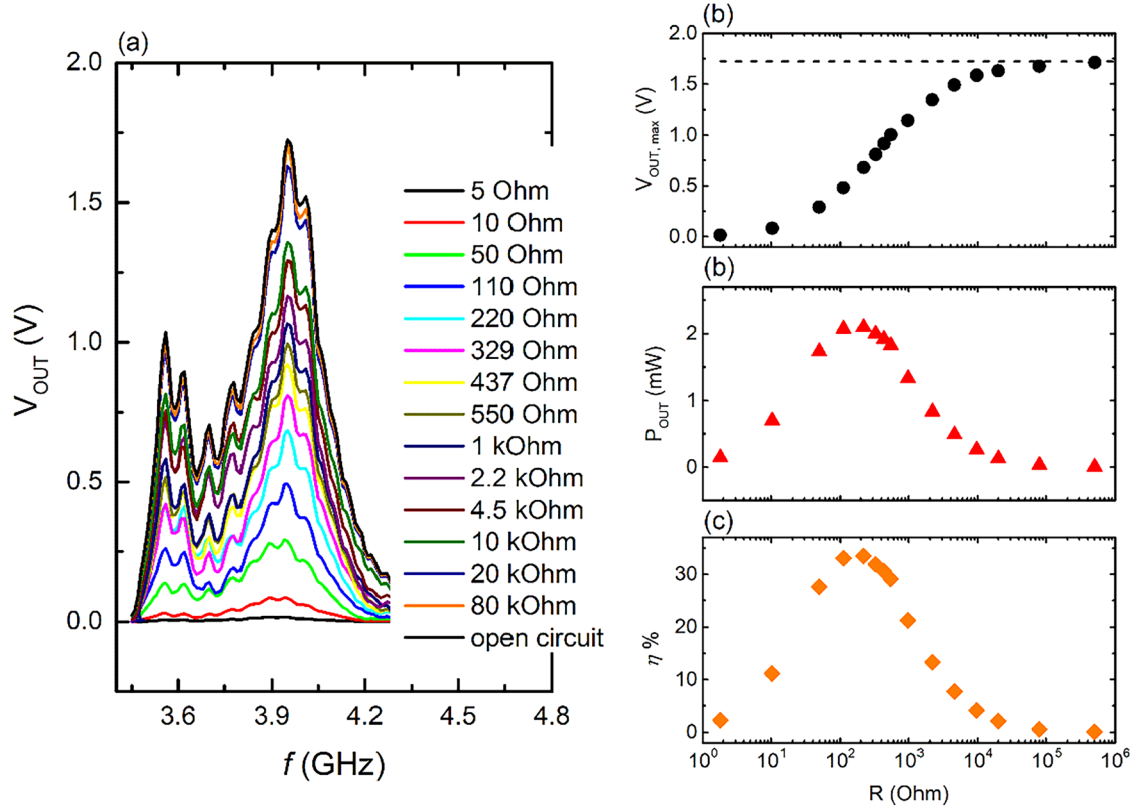


**FIG. 8.** (a)  $V_{OUT}$  vs frequency for various resistance loadings. (b) Peak value of  $V_{OUT}$  as a function of resistance loading  $R$ , as extracted from panel. Dash line corresponds to the open circuit voltage value (c). Output power  $P_{OUT}$  vs  $R$  and (d) harvesting efficiency  $\eta$  % vs  $R$ . Peak efficiency is observed for  $R \sim 200 \Omega$ .

CTM1 sample, as well as it is qualitatively similar to the behavior of FFF printed metasurfaces.<sup>24</sup> The corresponding output power and efficiency of the CTM2 sample is demonstrated in Fig. 9(c). Maximum output power ( $P_{max} \sim 2$  mW) is obtained for resistance load of 1.5 k $\Omega$ , with a calculated efficiency of  $\sim 30\%$ . Maximum power output in such a high resistance load has been previously reported, in other microwave harvesters.<sup>55</sup> Comparing to the CTM1 sample, the efficiency is of the same level; however in the latter case, such an efficiency is obtained for higher resistance loading.

Regarding the resistance loading, in which maximum power output is achieved, it is found to be different between CTM1 and CTM2. On the other hand, resistance load of the CTM1 is of the same range as that obtained for cut-wire metasurface units (i.e.,  $\sim 500 \Omega$ ), regardless their different shapes.<sup>24</sup> In electronic circuits, maximum power output values are obtained, when impedance matching is achieved, that is when the input impedance and the output impedance of a given electrical load are designed to reduce signal reflection and maximize the power transferred to the electric load.<sup>56</sup> A metasurface can be considered as an RLC electronic circuit, consisting of a resistor  $R$ , a capacitor  $C$  and an inductor  $L$ , connected in series. Such a circuit possesses an input impedance

$Z_{in} = \sqrt{R^2 + \left(j\omega L - \frac{1}{j\omega C}\right)^2}$ . Variation of any of the three  $R$ ,  $L$ ,  $C$  parameters would result in the variation of the total input impedance. Moreover, maximum power output, of such circuits, requires a resistance load with output impedance  $Z_{out}$ , matched to the corresponding  $Z_{in}$ . On resonance, the imaginary part of the input impedance is zeroed out. Thus, the load impedance is used to modify the real part of  $Z_{in}$  and achieve impedance matching with the input wave. Considering the above discussion, different resistance loads obtained for CTM1 and CTM2 could be attributed to the ground plane that existed in the latter. Ground plane existence, most probably results in increasing of the total input impedance  $Z_{in}$  of the metasurface unit, and consequently the required output impedance  $Z_{out}$  of the load should be increased so that impedance matching is achieved.

Other metasurface harvesters,<sup>41–43,57</sup> with toroidal geometry, possess higher efficiencies; therefore, the hereby obtained efficiency values are much lower. Furthermore, compared to other complementary harvesting metasurfaces' efficiency<sup>21,22,27–29,58</sup> ( $>80\%$ ), hereby obtained efficiencies are still inferior. Nevertheless, among other microwave energy harvesting metasurface arrays,<sup>25,45,59</sup> our

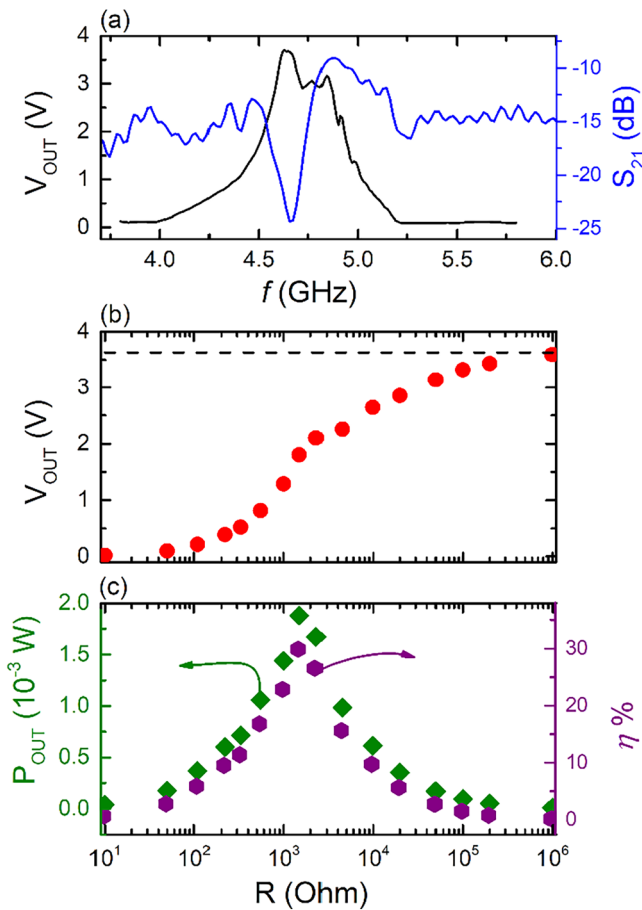


**FIG. 9.** (a) Open circuit voltage vs frequency for the CMT2 sample (black line). A clear peak is observed at the frequency where the metasurface absorbs (blue line). (b)  $V_{OUT}$  vs resistance loading. Black dashed line corresponds to  $V_{OC}$  value. (c) Peak value of  $V_{OUT}$  as a function of resistance loading  $R$ , as extracted from panel. Dash line corresponds to the open circuit voltage value. (c) Output power  $P_{OUT}$  and harvesting efficiency  $\eta\%$  with respect to the resistance loading  $R$ . Peak efficiency is observed for  $R \sim 1.5$  k $\Omega$ .

toroidal CNC-printed complementary metasurface units exhibit comparable or even superior harvesting performance.

It is noteworthy that the obtained efficiency of the investigated toroidal metasurface harvesters can be considered as underestimated. Several factors related to the performance of our harvesters are not optimized. First of all, the simple rectifying circuit, used for the RF-to-DC conversion, is not the optimal one, resulting in the suppression of the harvester performance. In general, special RF-to-DC converters are designed and developed, individually dedicated to each microwave harvesting system, so that they suppress parasitic effects, leading to the optimization of the rectifier performance and consequently to the maximization of the efficiency of the harvesting device.<sup>27,29,60–62</sup> However, rectifiers themselves possess a limited efficiency, which, in practice, is always lower than 100%, reducing the performance of the harvester. In the current

investigation, the rectifying circuit consists of a Schottky diode, and obviously it is not optimized to the requirements of the harvester. Therefore, the efficiency of the rectifying circuit itself is possibly very low, reducing further the performance of the toroidal harvesters. Nonetheless, such a simple rectifying circuit has been previously chosen,<sup>24</sup> for 3D-printed cut-wire metasurfaces, to successfully demonstrate their harvesting performance in the microwave regime. Furthermore, in the current investigation, harvesters consist of one single metasurface, while in other reports, harvesters consist of metasurface arrays, which could also contribute to their total performance. Considering all the above, it is obviously shown that the obtained efficiency for the investigated toroidal harvesters can be considered as underestimated, and further research is required toward their performance enhancement. Nevertheless, such research is out of the scope of the current study.

#### IV. SUMMARY AND CONCLUSIONS

In the current study, complementary metasurfaces, with toroidal topology, have been engraved, utilizing the CNC method. Both shape and dimensions of the metasurface are consistent with our previous theoretical and experimental investigation. The engraving process has also been previously used, for the construction of complementary metasurface sensors, dedicated for water quality control against detergents and fertilizers. Metasurfaces were engraved on metallized FR-4 surfaces. Two different FR-4 surfaces were used; a single-side Cu coated and a double -side Cu coated one. Thus, two different metasurfaces were formatted, i.e., one with a back conducting plate acting as a ground plane and another without the ground plane.

Both of them are characterized regarding their shape and dimensions. Compared to the initial design imported to the CNC router software, the dimensions measured in the developed metasurface are in a rather good agreement. Furthermore, the metasurface is well shaped, nevertheless with round corners. Therefore, the CNC process could be used for the production of complementary metasurfaces; however, optimization of the process will increase the quality of the produced samples.

Electromagnetic characterization of the grown metasurfaces reveals their strong electromagnetic response in certain frequencies, predicted by corresponding theoretical simulations. Moreover, their electromagnetic behavior with respect to the angle of the incident wave was studied and found to be consistent with theoretical predictions.

Harvesting behavior of the metasurfaces was extensively studied, through various experiments. Open circuit voltage as high as 3.6 and 1.75 V were measured, for the metasurfaces with and without the ground plane. These voltage values were observed in the frequencies where the metasurface resonate. Furthermore, open circuit voltage increases with increasing the power incident the metasurface, reaching saturation above a threshold value. All these experimental results clearly demonstrate the microwave energy harvesting performance of the engraved metasurfaces. By incorporating proper resistance loading, a maximum power output is obtained, leading to a corresponding harvesting efficiency of more than 30% for both studied metasurfaces. Such an efficiency is still

03 June 2024 09:26:02

inferior comparing to other metasurfaces with the toroidal geometry; however, it is comparable or even superior than other complementary metasurface harvesters. Furthermore, optimization of the rectification process, used hereby, as well as the construction of corresponding metasurface arrays, could also result in significant improvement of the harvesting efficiency, of the studied metasurfaces.

All in all, engraved complementary metasurfaces are quite promising candidates for energy harvesting applications in the microwave band.

## SUPPLEMENTARY MATERIAL

See the [supplementary material](#) for Figs. S1–S5, in which supporting experimental data are provided regarding the electromagnetic response of the hereby studied metasurfaces, as well as their energy harvesting behavior. In particular: Fig. S1 on  $S_{11}$  vs  $f$  spectrum for CTM1 sample. (b)  $S_{11}$  vs  $f$  spectrum for CTM2 sample; Fig. S2 for different angles that the metasurface can be turned, with respect to the incident wave, namely, delta theta and phi; Fig. S3 for theoretical simulations for CTM1 sample; Fig. S4 for theoretical simulations for CTM2 sample; and Fig. S5 for energy harvesting experimental results, with respect to the incident wave angle, for CTM2 sample.

## ACKNOWLEDGMENTS

This work was funded by the project “METAmaterial-based ENERGY autonomous systems (META-ENERGY) (Project ID 2936)” which is implemented under the 2nd Call for H.F.R.I. “Research Projects to Support Faculty Members & Researchers” funded by the Operational Programme “Competitiveness, Entrepreneurship and Innovation” (NSRF 2014–2020). O.T. and A.T. acknowledge support by the Hellenic Foundation for Research and Innovation (H.F.R.I.) under the “2nd Call for H.F.R.I. Research Projects to support Post-doctoral Researchers” (Project No. 916, PHOTOSURE).

## AUTHOR DECLARATIONS

### Conflict of Interest

The authors have no conflicts to disclose

## Author Contributions

**G. Fanourakis:** Data curation (equal); Formal analysis (equal); Investigation (equal); Methodology (equal); Writing – original draft (lead); Writing – review & editing (lead). **P. Markaki:** Data curation (equal); Formal analysis (equal); Investigation (equal); Writing – original draft (supporting); Writing – review & editing (supporting). **A. Theodosi:** Data curation (equal); Formal analysis (equal); Investigation (equal); Methodology (equal); Software (lead); Validation (equal); Writing – review & editing (equal). **O. Tsilipakos:** Data curation (equal); Formal analysis (equal); Investigation (equal); Software (equal); Validation (equal); Writing – original draft (supporting); Writing – review & editing (equal). **Z. Viskadourakis:** Conceptualization (equal); Investigation (equal); Methodology (equal); Project administration (equal); Supervision

(equal); Validation (equal); Visualization (equal); Writing – original draft (equal); Writing – review & editing (equal). **G. Kenanakis:** Conceptualization (equal); Data curation (equal); Formal analysis (equal); Funding acquisition (equal); Methodology (equal); Project administration (equal); Resources (equal); Supervision (equal); Validation (equal); Visualization (equal); Writing – original draft (equal); Writing – review & editing (equal).

## DATA AVAILABILITY

The data that support the findings of this study are available from the corresponding authors upon reasonable request.

## REFERENCES

- 1I. V. Shadrivov and D. N. Neshev, *World Scientific Handbook of Metamaterials Plasmon* (World Scientific, 2017), pp. 387–418.
- 2S. B. Glybovski, S. A. Tretyakov, P. A. Belov, Y. S. Kivshar, and C. R. Simovski, *Phys. Rep.* **634**, 1 (2016).
- 3G. Li, S. Zhang, and T. Zentgraf, *Nat. Rev. Mater.* **2**, 17010 (2017).
- 4R. Alaei, M. Albooyeh, and C. Rockstuhl, *J. Phys. D: Appl. Phys.* **50**, 503002 (2017).
- 5C. M. Soukoulis, S. Linden, and M. Wegener, *Science* **315**, 47 (2007).
- 6S. S. Bukhari, J. (Yiannis) Vardaxoglou, and W. Whittow, *Appl. Sci.* **9**, 2727 (2019).
- 7T. Chen, S. Li, and H. Sun, *Sensors* **12**, 2742 (2012).
- 8Y.S. Choudhary and N. Gomathi, *Advanced Materials for Electromagnetic Shielding* (Wiley, 2018), pp. 367–391.
- 9D. C. Zografopoulos and O. Tsilipakos, *Mater. Adv.* **4**, 11 (2023).
- 10J. Zeng, X. Wang, J. Sun, A. Pandey, A. N. Cartwright, and N. M. Litchinitser, *Sci. Rep.* **3**, 2826 (2013).
- 11H. Yang, T. Yu, Q. Wang, and M. Lei, *Sci. Rep.* **7**, 5441 (2017).
- 12N. Suresh Kumar, K. C. Naidu, P. Banerjee, T. Anil Babu, and B. Venkata Shiva Reddy, *Crystals* **11**, 518 (2021).
- 13O. Tsilipakos and T. Koschny, *Phys. Rev. B* **107**, 165408 (2023).
- 14T. Gric and E. Rafailov, *Optik* **254**, 168678 (2022).
- 15M. Yuan, Z. Cao, J. Luo, and X. Chou, *Micromachines* **10**, 48 (2019).
- 16Z. Chen, B. Guo, Y. Yang, and C. Cheng, *Phys. B* **438**, 1 (2014).
- 17M. Amiri, F. Tofigh, N. Shariati, J. Lipman, and M. Abolhasan, *IEEE Internet Things J.* **8**, 4105 (2021).
- 18A. A. G. Amer, S. Z. Sapuan, N. Nasimuddin, A. Alphones, and N. B. Zinal, *IEEE Access* **8**, 76433 (2020).
- 19D. Liu, W. Hong, T. S. Rappaport, C. Luxey, and W. Hong, *IEEE Trans. Antennas Propag.* **65**, 6205 (2017).
- 20E. Reyes-Vera, D. E. Senior, J. M. Luna-Rivera, and F. E. López-Giraldo, *TecnoLógicas* **21**, 9 (2018).
- 21B. Alavikia, T. S. Almoneef, and O. M. Ramahi, *Appl. Phys. Lett.* **107**, 033902 (2015).
- 22B. Alavikia, T. S. Almoneef, and O. M. Ramahi, *Appl. Phys. Lett.* **104**, 163903 (2014).
- 23G. T. Oumbé Tékam, V. Ginis, J. Danckaert, and P. Tassin, *Appl. Phys. Lett.* **110**, 083901 (2017).
- 24Z. Viskadourakis, E. Tamiolakis, O. Tsilipakos, A. C. Tasolamprou, E. N. Economou, and G. Kenanakis, *Crystals* **11**, 1089 (2021).
- 25M. Q. Dinh, T. Le Hoang, H. Tien Vu, N. T. Tung, and M. T. Le, *J. Phys. D: Appl. Phys.* **54**, 345502 (2021).
- 26B. Ghaderi, V. Nayyeri, M. Soleimani, and O. M. Ramahi, *IET Microw. Antennas Propag.* **12**, 2271 (2018).
- 27A. Benayad and M. Tellache, *Microelectron. J.* **125**, 105460 (2022).
- 28N. Ullah, M. S. Islam, A. Hoque, W. H. Yong, M. S. Soliman, S. Albadran, and M. T. Islam, *Eng. Sci. Technol.* **45**, 101473 (2023).

- <sup>29</sup>P. Lu, C. Song, and K. M. Huang, *IEEE Trans. Microw. Theory Tech.* **69**, 3452 (2021).
- <sup>30</sup>I. Grout, edited by I.B.T.-D.S.D. with Fpga. and Cpld. Grout (Newnes, Burlington, 2008), pp. 123–176.
- <sup>31</sup>I. Chtioui, F. Bossuyt, M. de Kok, J. Vanfleteren, and M. H. Bedoui, *IEEE Trans. Components Packag. Manuf. Technol.* **6**, 533 (2016).
- <sup>32</sup>O. Cakir, *J. Mater. Process. Technol.* **175**, 63 (2006).
- <sup>33</sup>Z. Viskadourakis, G. Fanourakis, E. Tamiolakis, A. Theodosi, K. Katsara, N. R. Vrithias, O. Tsilipakos, and G. Kenanakis, *Materials* **16**, 5290 (2023).
- <sup>34</sup>A.N. Nordin and A. Abd Manaf, edited by W.C. Mak and A.H.B.T.-M.B. Pui Ho (Academic Press, 2023), pp. 41–85.
- <sup>35</sup>H. Yao, S. Qiu, Y. Lv, S. Wei, A. Li, Z. Long, W. Wu, and X. Shen, *Sustainability* **15**, 6227 (2023).
- <sup>36</sup>S. Kumar, A. Nassehi, S. T. Newman, R. D. Allen, and M. K. Tiwari, *Robot. Comput. Integr. Manuf.* **23**, 667 (2007).
- <sup>37</sup>J. Meher, B. B. Nayak, A. Panda, R. Kumar, and A. K. Sahoo, *Mater. Today Proc.* **62**, 3983 (2022).
- <sup>38</sup>L. Xie, X. Chen, H. Yan, H. Xie, and Z. Lin, *J. Phys.: Conf. Ser.* **1646**, 012091 (2020).
- <sup>39</sup>F. Rabiei and S. Yaghoubi, *Mater. Today Commun.* **36**, 106482 (2023).
- <sup>40</sup>O. Tsilipakos, Z. Viskadourakis, A. C. Tasolamprou, D. C. Zografopoulos, M. Kafesaki, G. Kenanakis, and E. N. Economou, *Micromachines* **14**, 468 (2023).
- <sup>41</sup>M. A. Aldhaeabi and T. S. Almomneef, *Materials* **14**, 6242 (2021).
- <sup>42</sup>M. A. Aldhaeabi and T. S. Almomneef, *Electronics* **9**, 1985 (2020).
- <sup>43</sup>X. Duan, X. Chen, Y. Zhou, L. Zhou, and S. Hao, *IEEE Antennas Wirel. Propag. Lett.* **17**, 1617 (2018).
- <sup>44</sup>G. Kenanakis, K. C. Vasilopoulos, Z. Viskadourakis, N.-M. Barkoula, S. H. Anastasiadis, M. Kafesaki, E. N. Economou, and C. M. Soukoulis, *Appl. Phys. A* **122**, 802 (2016).
- <sup>45</sup>A. M. Hawkes, A. R. Katko, and S. A. Cummer, *Appl. Phys. Lett.* **103**, 163901 (2013).
- <sup>46</sup>R. Wang, D. Ye, S. Dong, Z. Peng, Y. Salamin, F. Shen, J. Huangfu, C. Li, and L. Ran, *IEEE Trans. Microw. Theory Tech.* **62**, 1080 (2014).
- <sup>47</sup>D. Wang and R. Negra, *IEEE Trans. Microw. Theory Tech.* **62**, 1080 (2014).
- <sup>48</sup>T. S. Almomneef, F. Erkmen, and O. M. Ramahi, *Sci. Rep.* **7**, 14656 (2017).
- <sup>49</sup>T. S. Almomneef and O. M. Ramahi, *Appl. Phys. Lett.* **106**, 153902 (2015).
- <sup>50</sup>F. Erkmen and O. M. Ramahi, *IEEE Trans. Microw. Theory Tech.* **69**, 4021 (2021).
- <sup>51</sup>O. M. Ramahi, T. S. Almomneef, M. AlShareef, and M. S. Boybay, *Appl. Phys. Lett.* **101**, 173903 (2012).
- <sup>52</sup>T. Tan, Z. Yan, H. Zou, K. Ma, F. Liu, L. Zhao, Z. Peng, and W. Zhang, *Appl. Energy* **254**, 113717 (2019).
- <sup>53</sup>M. Q. Qi, W. X. Tang, H. F. Ma, B. C. Pan, Z. Tao, Y. Z. Sun, and T. J. Cui, *Sci. Rep.* **5**, 9113 (2015).
- <sup>54</sup>M. Cansiz, D. Altinel, and G. K. Kurt, *Energy* **174**, 292 (2019).
- <sup>55</sup>A. Z. Ashoor, T. S. Almomneef, and O. M. Ramahi, *IEEE Trans. Microw. Theory Tech.* **66**, 1553 (2018).
- <sup>56</sup>T. L. Floyd, *Principles of Electric Circuits: Conventional Current Version* (Pearson Prentice Hall, 2007).
- <sup>57</sup>H.Y.A. Ajm and M.M. Bait-Suwailam, in *2022 International Conference on Electrical and Computing Technologies and Applications (ICECTA)*, p. 378 (2022).
- <sup>58</sup>A. Ghaneizadeh, K. Mafinezhad, and M. Joodaki, *AIP Adv.* **9**, 025304 (2019).
- <sup>59</sup>A. Z. Ashoor and O. M. Ramahi, *IEEE Trans. Microw. Theory Tech.* **67**, 1130 (2019).
- <sup>60</sup>M. A. Halimi, T. Khan, Nasimuddin, A. A. Kishk, and Y. M. M. Antar, *IEEE Microw. Mag.* **24**, 46 (2023).
- <sup>61</sup>S. A. Rotenberg, S. K. Podilchak, P. D. H. Re, C. Mateo-Segura, G. Goussetis, and J. Lee, *IEEE Trans. Microw. Theory Tech.* **68**, 1921 (2020).
- <sup>62</sup>C. Jin, J. Wang, D. Y. Cheng, K. F. Cui, and M. Q. Li, *J. Phys.: Conf. Ser.* **1168**, 022020 (2019).